Two-dimensional Vlasov solution for a collisionless plasma jet across transverse magnetic field lines with a sheared bulk velocity

Marius M. Echim[1,2,*]
[1]*Institut d'Aéronomie Spatiale de Belgique, Avenue Circulaire 3, B-1180 Brussels, Belgium*
[2]*Institute of Space Sciences, Atomiştilor 409, P.O. Box MG-23, R-77125 Bucharest, Romania*

Joseph F. Lemaire
Centre for Space Radiation, Université Catholique de Louvain, Chemin du Cyclotron 2, 1348 Louvain-la-Neuve, Belgium
(Received 25 May 2005; published 13 September 2005)

We consider a two-dimensional (2D) stationary stream of a collisionless plasma injected across an external stationary magnetic field and a background stagnant plasma. The solution is found by solving the Vlasov equation for each species (electrons and protons), the Maxwell-Ampere equation for the magnetic vector potential, and the equation of plasma quasineutrality for the electrostatic potential. The solution of the stationary Vlasov equation is given in terms of two constants of motion and one adiabatic invariant. The partial charge and current densities are given by analytical expressions of the moments of the velocity distribution functions for each particle species. The 2D distribution of the plasma bulk velocity, $V_x(y,z)$, is roughly uniform inside the jet. There is no plasma bulk flow in the direction of the magnetic field. Inside the boundary layer interfacing the jet and the stagnant plasma, the bulk velocity has gradients (i.e., *shears*) in the direction parallel as well perpendicular to the magnetic field. The parallel component of this gradient, $\nabla_{\parallel}V_{\perp}$, produces a nonzero electric field component parallel to the magnetic field lines, $\boldsymbol{E}\cdot\boldsymbol{B}\neq 0$. The parallel electric field within the transition layer is a basic element allowing plasma elements to be transported across magnetic field lines in astrophysical systems as well as in laboratory experiments where plasmoids are injected across magnetic fields.

DOI: 10.1103/PhysRevE.72.036405 PACS number(s): 52.65.Ff, 52.25.Xz, 52.27.Ep

I. INTRODUCTION

Plasma motion across magnetic field lines is a key mechanism for momentum and energy transport in astrophysical observations (e.g., Ref. [1]) and models [2] as well as in laboratory experiments (e.g., Refs. [3,4]) or fusion devices [5]. In this paper we focus our attention on the problem of a stationary, nonuniform collisionless plasma stream across magnetic field lines. We determine the plasma variables and fields inside the two-dimensional boundary layer forming at the interface between the moving plasma and the adjacent stagnant one.

One-dimensional solutions for tangential disconti nuities (TDs) interfacing two *stagnant* plasma regions with different temperatures and densities on both sides were studied previously by Sestero [6] for unidirectional magnetic field distributions and by Lemaire and Burlaga [7] for one-dimensional (1D) sheared magnetic field distributions. One-dimensional TD equilibrium solutions interfacing two separate plasma regions moving across unidirectional magnetic field distributions were investigated by Sestero [8] and Roth [9]. Vlasov equilibrium solutions for one-dimensional TDs with shears both of the magnetic field distribution and of the convection velocity have been described by Roth *et al.* [10] and Lee and Kan [11]. In these 1D kinetic models the plasma parameters (density, temperature, bulk velocity) and fields (magnetic and electric fields) vary only in the direction perpendicular to both the direction of the magnetic field and of the plasma bulk velocity. Echim [12] showed that the solutions proposed for steady-state one-dimensional TDs can be extended to the more general case of 2D kinetic solutions for a nonuniform plasma streaming across magnetic field lines with a sheared convection velocity. In the work of Echim [12] the plasma and fields distributions are not uniform in the direction perpendicular and parallel to the magnetic field lines.

In the following we describe this 2D kinetic solution for the sheared flow of collisionless plasma. The convection velocity is parallel to the x direction; the background magnetic field is parallel to the Oz direction, $\boldsymbol{B}_0\equiv(0,0,B_0)$, as illustrated in Fig. 1. The plasma variables and field are functions of y and z. Echim [12] has shown that internal plasma currents are then parallel to the x axis, producing thus diamagnetic field perturbations which are parallel to the $(y\text{-}z)$ plane. These magnetic perturbations add to background or external magnetic field, $\boldsymbol{B}_0$, to produce a total magnetic field $\boldsymbol{B}=(0,B_y(y,z),B_z(y,z))=(0,b_y(y,z),B_0+b_z(y,z))$, where $b_y(y,z)$ and $b_z(y,z)$ denote the magnetic perturbations produced by the internal plasma currents.

The plasma jet in our model has a bulk velocity (or convection velocity) whose only nonvanishing component is parallel to the Ox direction: $\boldsymbol{V}=(V_x,0,0)$ with $\partial V_x/\partial y\neq 0$, $\partial V_x/\partial z\neq 0$, and $\partial V_x/\partial x=0$. Therefore this study is restricted to the case when there is no bulk plasma transport in the direction of the magnetic field, nor in the Oz or Oy directions. It is assumed that an external driver sustains the nonuniform and stationary plasma flow across the external magnetic field $\boldsymbol{B}_0$. This driver can be an initial push imparted to the particles by a plasma gun in laboratory experiments, the inertia of solar and stellar winds, or the drag due to neutral

*Electronic address: marius.echim@oma.be

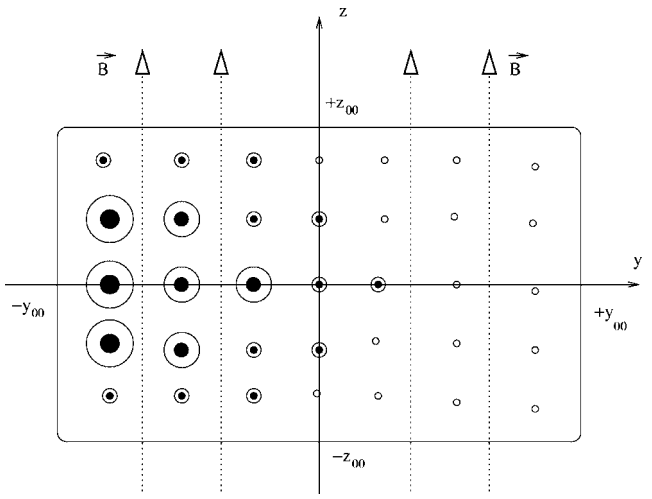

FIG. 1. Cross section of a sheared 2D plasma flow across an external B field, $\boldsymbol{B}_0$, which is parallel to the Oz axis: $\boldsymbol{V}$, the plasma bulk velocity (vectors pointing out of the sheet of paper) is everywhere parallel to the positive x direction; $V_x(y,z)$ is a function of y and z. It is represented by circles whose diameter is proportional to $V_x(y,z)$. Dotted lines illustrate the distribution of the external magnetic field $\boldsymbol{B}_0$. The diamagnetic field perturbations produced by the small current density circulating in the boundary layer along the surface of the plasma jet are not shown but are self-consistently calculated in our model.

winds as in the topside ionosphere of the Earth. The problem is stationary and $\partial/\partial t=0$ throughout this study. These approximations may appear as rather restrictive, but this work is among the most complicated situations solved for 2D sheared plasma flows. It is a step ahead toward the ultimate goal of kinetic modeling 3D plasma flows.

The paper is organized as follows. Section II describes the solution found for the Vlasov equation. Section III gives the analytic expressions of the moments of the velocity distribution function (i.e., density, flux of particles). The electron and proton densities and fluxes are needed to compute the self-consistent electromagnetic potentials, $\Phi(y,z)$ and $A_x(y,z)$. Section IV outlines the numerical method used to solve the equations for the electromagnetic potentials. It includes also a cross checking of the method in the case of a 1D tangential discontinuity. The results are compared to those already published in the literature. Section V shows the numerical results obtained for a 2D layer formed at the interface between a moving cold plasma stream and a stagnant plasma both with the same temperature and density at large distances. Finally, Sec. VI includes a discussion on the aspects of our model that are relevant to the problem of nonuniform plasma flows across magnetospheric magnetic fields.

II. SOLUTION OF THE VLASOV EQUATION

The solution for the problem of a stationary 2D flow across an external magnetic field is sought in the framework of the kinetic theory of collisionless plasma. Only two plasma species, electrons (charge: $q_e=-e=-1.6022\times10^{-19}$ C; mass: $m_e=9.1094\times10^{-31}$ kg) and protons (charge: $q_p=+e$; mass: $m_p=1.6726\times10^{-27}$ kg), will be considered. Each species (indexed with α) is characterized by a velocity distribution function (VDF), $f_\alpha(\boldsymbol{r},\boldsymbol{v})$, that satisfies the stationary Vlasov equation:

$$\boldsymbol{v}\cdot\frac{\partial f_\alpha}{\partial \boldsymbol{r}}+\frac{q_\alpha}{m_\alpha}(\boldsymbol{E}+\boldsymbol{v}\times\boldsymbol{B})\cdot\frac{\partial f_\alpha}{\partial \boldsymbol{v}}=0. \tag{1}$$

It is known that the characteristic curves of Eq. (1) are the trajectories of the particle with mass m_α and charge q_α injected into the electromagnetic field distribution, $\boldsymbol{E}(\boldsymbol{r})$ and $\boldsymbol{B}(\boldsymbol{r})$ [13]. Thus instead of solving the PDE (1) in the six-dimensional space $(\boldsymbol{r},\boldsymbol{v})$ one can write the solution as any positive, real function of the constants of motion of the particle in this steady state electromagnetic field. In the following we describe the method to transform the VDF of each species from the velocity space into the space of the constants of motion.

A. Constants of motion

The plasma jet is described in a Cartesian coordinates system. In the case of stationary E and B fields, H, the Hamiltonian (or total energy) of the charged particles, is a constant of motion:

$$H=\frac{m_\alpha}{2}(v_x^2+v_y^2+v_z^2)+q_\alpha\phi(y,z). \tag{2}$$

Since the potentials Φ and $\boldsymbol{A}$ do not depend on x, the x coordinate is *ignorable*. Thus the corresponding component of the canonical momentum, p_x, is a second constant of motion:

$$p_x=m_\alpha v_x+q_\alpha A_x(y,z). \tag{3}$$

The VDF is a function of the three velocity components, v_x,v_y,v_z. To complete the transformation from the 3D space of velocities into the space of constants of motion a third constant of motion is needed. Note that in the one-dimensional models of TDs, where the plasma parameters and E and B fields components were independent of z and did vary only with the y coordinate the third constant of motion was given by $p_z=m_\alpha v_z+q_\alpha A_z(y)$. Since in our 2D problem we consider that Φ and $\boldsymbol{A}$ depend also on the z coordinate, the invariance of p_z is lost. The magnetic moment of the particle α,μ_α, which is an adiabatic invariant under certain conditions, will be here used as the third constant of motion. It will be in fact used to compute the Jacobian of the transformation from the velocity space to the space of the constants of motion.

The conditions under which the magnetic moment of the particles is adiabatic invariant are the Alfven conditions [14,15]. This implies that $r_{L\alpha}|\nabla B|\ll B$, where $r_{L\alpha}$ is the Larmor radius of the particle α. The zero order drift velocity $\boldsymbol{U}_{Ex}$ has only one nonvanishing component, in the Ox direction. The total magnetic field, $\boldsymbol{B}$, is mainly parallel to the Oz direction ($B_y\ll B_z$), thus the magnetic moment is equal to

$$\mu_\alpha = \frac{m_\alpha[(v_x - U_E)^2 + v_y^2]}{2B}. \quad (4)$$

The adiabatic invariant μ was used in the past to construct one-dimensional kinetic solutions for the ionized gas flowing out of the solar corona as well as out of the terrestrial topside ionosphere [16–18]. In these earlier kinetic models the bulk velocity was assumed to be parallel to the magnetic field lines and has no component in the direction normal to the given background magnetic field. We propose here a 2D kinetic solution that combines the kinetic solutions developed for respectively the 1D kinetic models of TDs and the 1D kinetic exospheric models of the solar and polar winds.

B. Boundary conditions for f_α

Any real, positive function, $f_\alpha(H, p_x, \mu_\alpha)$ is a solution of Eq. (1). From the infinite number of choices one must select those VDFs that satisfy the boundary conditions describing the problem of interest. The solutions of the Vlasov and Maxwell equations will be computed inside the rectangle Γ defined by $[-y_\infty, +y_\infty] \times [-z_\infty, +z_\infty]$. Here $-y_\infty, +y_\infty, -z_\infty, +z_\infty$ take finite values still large compared to the electron Larmor radius. The boundary conditions that must be satisfied by f_α are derived from the following constraints on the plasma flow at the edges of the 2D domain:

(i) at the right hand side edge, $y = +y_\infty$, the plasma is at rest, $V = 0$;

(ii) at the left hand side edge, $y = -y_\infty$, the plasma is in motion in the x direction, the only nonvanishing component of the bulk velocity depends on the z coordinate,

$$\lim_{y \to -y_\infty} V_x = V_L(z);$$

(iii) at the bottom edge, $z = -z_\infty$, the plasma is in motion with a nonuniform velocity depending on the y coordinate,

$$\lim_{z \to -z_\infty} V_x = V_B(y);$$

the plasma velocity on the lower boundary has to satisfy the additional conditions

$$\lim_{y \to -y_\infty} V_B(y) = V_L(-z_\infty), \quad \lim_{y \to +y_\infty} V_B(y) = 0;$$

(iv) at the top edge, $z = +z_\infty$, the plasma has also a nonuniform velocity depending on the y coordinate,

$$\lim_{z \to +z_\infty} V_x = V_T(y),$$

with the additional constraints

$$\lim_{y \to -y_\infty} V_T(y) = V_L(+z_\infty), \quad \lim_{y \to +y_\infty} V_T(y) = 0.$$

In addition to the above boundary conditions, we expect that Eq. (1) gives a profile for the plasma bulk velocity $V_x(y,z)$ such that the gradient $\nabla_\parallel V_x$ in the direction parallel to the total magnetic field (external B_0 field + the diamagnetic b-field contribution due to the plasma currents) is different from zero: $\boldsymbol{B} \cdot \nabla V_x \neq 0$ unlike in ideal magnetohydrodynamics (MHD) flows where $\boldsymbol{E} \cdot \boldsymbol{B} = 0$ and therefore $\boldsymbol{B} \cdot \nabla V_x = 0$.

We consider that the nonmoving plasma at the right hand side edge, $y = +y_\infty$, is in thermal equilibrium and the corresponding boundary value of f_α is equal to an isotropic Maxwellian distribution defined by

$$f_{\alpha 1}(v_x, v_y, v_z) = N_{\alpha 1}\left(\frac{m_\alpha}{2\pi K T_{\alpha 1}}\right)^{3/2} e^{-m_\alpha (v_x^2 + v_y^2 + v_z^2)/2KT_{\alpha 1}}. \quad (5)$$

$N_{\alpha 1}$ and $T_{\alpha 1}$ are the density and temperature of the stagnant populations. On the other three edges of the two-dimensional domain Γ the VDF will give an average velocity in the x direction that is nonuniform. Therefore we define a displaced Maxwellian VDF with a constant velocity V_0:

$$f_{\alpha 2}(v_x, v_y, v_z) = N_{\alpha 2}\left(\frac{m_\alpha}{2\pi K T_{\alpha 2}}\right)^{3/2} e^{-m_\alpha [(v_x - V_0)^2 + v_y^2 + v_z^2]/2KT_{\alpha 2}} \quad (6)$$

that is also a solution of the Vlasov equation (1). The boundary values of f_α on the bottom, left, and top edges will then be defined as a linear combination of the two functions (5) and (6).

The two VDFs, $f_{\alpha 1}$ and $f_{\alpha 2}$, can be transformed from the velocity space (v_x, v_y, v_z) into the space of the constants of motion (H, p_x, μ_α):

$$f_{\alpha 1}(H, p_x, \mu_\alpha) = N_{\alpha 1}\left(\frac{m_\alpha}{2\pi K T_{\alpha 1}}\right)^{3/2} e^{-H/KT_{\alpha 1}}, \quad (7)$$

$$f_{\alpha 2}(H, p_x, \mu_\alpha) = N_{\alpha 2}\left(\frac{m_\alpha}{2\pi K T_{\alpha 2}}\right)^{3/2} e^{-(H - p_x V_0 + (1/2) m_\alpha V_0^2)/KT_{\alpha 2}}. \quad (8)$$

Note that neither $f_{\alpha 1}$ nor $f_{\alpha 2}$ directly depend on μ_α, but the Jacobian of the transformation does. The new expressions of $f_{\alpha 1}$ and $f_{\alpha 2}$ depend implicitly on the spatial coordinates (y,z) via the electromagnetic potentials, $\Phi(y,z)$ and $A_x(y,z)$, that enter in the definitions of the two constants of motion H and p_x. Thus $f_{\alpha 2}$ from Eq. (8) gives the expected boundary VDF on the left edge of Γ when the following condition is satisfied:

$$\lim_{y \to -y_\infty} A_x(y,z) = A_{xL}(z),$$

where $A_{xL}(z)$ is the boundary condition to be imposed on the magnetic vector potential on the left boundary of the domain Γ.

The VDF on the bottom ($f_{\alpha B}$) and top ($f_{\alpha T}$) edges of the domain have to be determined in such a way that the following conditions are satisfied:

$$\lim_{y \to -y_\infty} f_{\alpha B} = f_{\alpha 2}, \quad \lim_{y \to +y_\infty} f_{\alpha B} = f_{\alpha 1}, \quad (9)$$

$$\lim_{y \to -y_\infty} f_{\alpha T} = f_{\alpha 2}, \quad \lim_{y \to +y_\infty} f_{\alpha T} = f_{\alpha 1}. \quad (10)$$

A VDF that has this desired asymptotic behavior is precisely the Vlasov solution proposed for the 1D kinetic models of tangential discontinuities [8,10]. Following Sestero [8] the boundary value on the bottom edge can be written as

TABLE I. Boundary values of the velocity distribution function f_α, of the plasma bulk velocity V_x, and of the magnetic vector potential A_x. The functions $f_{\alpha 1}$, $f_{\alpha 2}$, and $f_{\alpha B}$ are defined, respectively, by Eq. (7), (8), and (11).

Boundary	$y=-y_\infty$	$y=+y_\infty$	$z=-z_\infty$	$z=+z_\infty$
f_α	$f_{\alpha 1}$	$f_{\alpha 2}$	$f_{\alpha B}$	$f_{\alpha B}$
V_x	$V_L(z)$	0	$V_B(y)$	$V_T(y)$
A_x	$B_0 y_\infty + \zeta(z)$	$-B_0 y_\infty$	$-B_0 y$	$-B_0 y$

$$f_{\alpha B}(p_x,H) = \eta\left(-b_\alpha \frac{p_x}{\sqrt{m_\alpha K T_{\alpha 1}}}\right) f_{\alpha 1}(p_x,H) + \eta\left(b_\alpha \frac{p_x - m_\alpha V_0}{\sqrt{m_\alpha K T_{\alpha 2}}}\right) f_{\alpha 2}(p_x,H), \quad (11)$$

where $b_\alpha = \mathrm{sgn}(q_\alpha)$,[1] η is the Heaviside step function,[2] and the functions $f_{\alpha 1}(p_x,H)$ and $f_{\alpha 2}(p_x,H)$ are defined by Eqs. (7) and (8). We will restrict this study to the case where the VDF on the top edge takes the same boundary value as on the bottom edge: $f_{\alpha T}(p_x,H) = f_{\alpha B}(p_x,H)$.

We also choose the reference frame such that at the bottom and top edges the only nonvanishing component of the magnetic field is positive and equal to the external magnetic field ($B_0 > 0$). Thus the VDF defined in Eq. (11) satisfies the conditions (9) and (10) since

$$\lim_{y \to +y_\infty} \eta\left(\pm b_\alpha \frac{p_x}{\sqrt{m_\alpha K T_{\alpha 1}}}\right) = \eta(\mp 1), \quad (12)$$

$$\lim_{y \to -y_\infty} \eta\left(\pm b_\alpha \frac{p_x}{\sqrt{m_\alpha K T_{\alpha 1}}}\right) = \eta(\pm 1).$$

A summary of the boundary values of f_α is given in Table I.

C. 2D solution

Expanding previous one-dimensional tangential discontinuities models with perpendicular drift velocities [8,10] we seek here to extend them to two dimensions. We construct a 2D Vlasov equilibrium model based on the VDF determined by Eqs. (7), (8), (11).

Since $f_{\alpha B}$ given in Eq. (11) is a function of the constants of motion only, it is necessarily a solution of the Vlasov equation (1) not only on the lower and upper boundaries but also in the whole 2D domain Γ. Although its analytic expression is similar to the solution postulated for one-dimensional TDs, the electromagnetic potentials in the definitions of the constants of motion are now functions of y and z, not only on y as in earlier TDs models. Thus an admissible solution of the Vlasov equation that satisfies the boundary conditions described above is

$$f_\alpha(H,p_x,\mu_\alpha) = f_{\alpha B}, \quad (13)$$

where $f_{\alpha B}$ is defined by Eq. (11).

[1] $\mathrm{sgn}(q_\alpha < 0) = -1$, $\mathrm{sgn}(q_\alpha > 0) = +1$.
[2] $\eta(x<0)=0$, $\eta(x \geqslant 0)=1$.

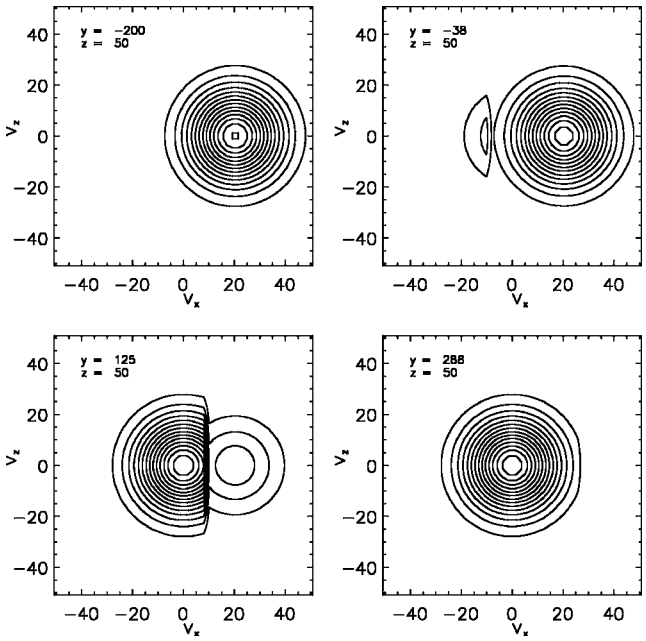

FIG. 2. Isocontours of the VDF of protons, $f_p(y,z,v_x,v_y,v_z)$, the solution of the Vlasov equation given by Eqs. (11) and (13). The isocontours are plotted in the plane of the velocity space defined by $v_y=0$ for different positions (y,z) in the plasma jet which is parallel to the Ox axis. Note the transition of the VDF from the displaced Maxwellian f_{p2} (at the left hand side edge—upper left panel), to the (stagnant) isotropic Maxwellian f_{p1} (at the right hand side edge—lower right panel). The electrostatic and magnetostatic potentials used to determine spatial distribution of the VDF are discussed in Sec. V.

This solution is not unique. An infinite number of other choices are possible. Our choice is dictated by convenience; indeed it enables us to obtain analytical expressions for the moments of the VDF, and the VDF itself is piecewise Maxwellian. The Heaviside step functions in Eq. (11) were also chosen on grounds of mathematical simplicity. Other, smoother functions can be also used (as in Refs. [10,11]) without altering the relevance of the results outlined below. Furthermore, the solution is valid for those E and B fields that satisfy the Alfven conditions and the condition that $\boldsymbol{B}$ is mainly aligned with the z direction, i.e., $|\boldsymbol{b}| \ll |\boldsymbol{B}_0|$.

A first example of the VDF is illustrated in Fig. 2. In these graphs the velocity distribution function of the protons is transformed back into the velocity space (v_x,v_y,v_z). The four panels of Fig. 2 illustrate 2D sections of the 3D velocity space (v_x,v_y,v_z) at four different points in the plasma jet advancing parallel to the Ox axis. One can note the transition of the VDF of the protons from the displaced Maxwellian f_{p2} (on the left hand side boundary, $y=-200$, $z=50$) to the isotropic Maxwellian f_{p1} (on the right hand side boundary, $y=+288$, $z=50$).

III. ELECTROMAGNETIC POTENTIALS: MOMENTS OF THE VDF

As consequence of the assumptions made on the flow ($\partial/\partial t = 0$, $\partial/\partial x = 0$) the electromagnetic field components are

$$\boldsymbol{E} \equiv (E_0, E_y(y,z), E_z(y,z)), \quad \boldsymbol{B} \equiv (0, B_y(y,z), B_z(y,z)), \tag{14}$$

where E_0 is a constant equal to zero since the plasma flow is everywhere aligned with the Ox direction and its bulk velocity is independent of x and of the time t. Without loss of generality the magnetic field distribution (14) can be obtained from a magnetic vector potential whose only nonvanishing component is A_x. Thus the two electromagnetic potentials are solutions of the Maxwell's equations,

$$\frac{\partial^2 \Phi}{\partial y^2} + \frac{\partial^2 \Phi}{\partial z^2} = -\frac{1}{\epsilon_0} \sum_\alpha \rho_\alpha(y,z), \tag{15}$$

$$\frac{\partial^2 A_x}{\partial y^2} + \frac{\partial^2 A_x}{\partial z^2} = -\mu_0 \sum_\alpha j_{\alpha x}(y,z). \tag{16}$$

The partial charge density ρ_α and current density $\boldsymbol{j}_\alpha$ are derived from the moments of the velocity distribution function of each species. The general expression for the moment of rst order is given by the triple integration over velocity space:

$$Q_\alpha^{rst}(\boldsymbol{r}) = \int\int\int v_x^r v_y^s v_z^t f_\alpha(x,y,z,v_x,v_y,v_z) d^3\boldsymbol{v}. \tag{17}$$

Since we specified the VDF in terms of the constants of motion, its moments are computed by a triple integration in the space (H, p_x, μ_α):

$$Q_\alpha^{rst}(\boldsymbol{r}) = 4 \int_{-\infty}^{+\infty} \int_0^{+\infty} \int_0^{+\infty} \Big([v_x(p_x,H,\mu_\alpha)]^r [v_y(p_x,H,\mu_\alpha)]^s \times [v_z(p_x,H,\mu_\alpha)]^t f_\alpha(p_x,H,\mu_\alpha) \left| \frac{D(v_x,v_y,v_z)}{D(p_x,H,\mu_\alpha)} \right| \Big) \times d\mu_\alpha dH dp_x, \tag{18}$$

where $|D(v_x,v_y,v_z)/D(p_x,H,\mu_\alpha)|$ is the Jacobian of the transformation from the (v_x,v_y,v_z) space to the (p_x,H,μ_α) space. The factor 4 in front of the integrals is due to the summation of the integrals when both s and t are even. As a consequence of the symmetry of the VDF whenever one of the two exponents s or t is odd the corresponding moment is equal to zero:

$$Q_\alpha^{rst} = 0 \quad (\text{for } s \text{ or } t \text{ odd}).$$

A detailed discussion on the integration over the four quadrants of the (v_y,v_z) subspace mapped into the (H,p_x,μ) space, is given by Echim [12].

In the expression (18) the three components of the velocity, v_x, v_y, v_z, are replaced by the corresponding functions of the constants of motion according to the definitions (2)–(4) The Jacobian of the transformation from the variables (H,p_x,μ) to (v_x,v_y,v_z) is equal to

$$\mathcal{J} = \left| \frac{D(v_x,v_y,v_z)}{D(H,p_x,\mu)} \right| = \frac{\sqrt{B}}{2m_\alpha^2 \sqrt{\mu - \mu_{c\alpha}} \sqrt{H - H_{c\alpha}}},$$

where the functions $H_{c\alpha}$ and $\mu_{c\alpha}$ are defined by

$$H_{c\alpha}(p_x,\mu) = \mu_\alpha B + (p_x - q_\alpha A_x) U_E + q_\alpha \Phi - \frac{m_\alpha U_E^2}{2}, \tag{19}$$

$$\mu_{c\alpha}(p_x) = \frac{m_\alpha}{2B} \left(\frac{p_x - q_\alpha A_x}{m_\alpha} - U_E \right)^2 \tag{20}$$

with $\boldsymbol{U}_E = (\boldsymbol{E} \times \boldsymbol{B})/B^2$. The conditions for the Jacobian to be real and finite,

$$H > H_{c\alpha}, \tag{21}$$

$$\mu_\alpha > \mu_{c\alpha}, \tag{22}$$

are equivalent to the conditions of accessibility of particles in the velocity space. The accessibility conditions for various profiles of the electric potential have been discussed in Refs. [16,19,20].

The charge density of each plasma species is found by computing the zero order moment of the VDF:

$$\rho_\alpha = q_\alpha Q_\alpha^{000}. \tag{23}$$

The current density is computed from the first order moments of the VDF. Only $j_{x\alpha}$ is different from zero:

$$j_{x\alpha} = q_\alpha n_\alpha u_\alpha = q_\alpha Q_\alpha^{100}, \tag{24}$$

where u_α is the average velocity of species α. The plasma bulk velocity is equal to the center of mass speed and is computed from

$$V_x(y,z) = \frac{m_p Q_p^{100}(\Phi,A_x) + m_e Q_e^{100}(\Phi,A_x)}{m_p Q_p^{000}(\Phi,A_x) + m_e Q_e^{000}(\Phi,A_x)}. \tag{25}$$

The analytical expressions of the charge and currents density are given in Appendix A. As a consequence of the large mass of the protons the second terms in the numerator and denominator of Eq. (25) can be neglected and the bulk velocity of plasma is almost equal to that of the protons. Note that in this kinetic model the average velocity of the electrons is not equal to that of the ions as assumed in single fluid MHD approximation.

IV. NUMERICAL METHOD: VERIFICATION FOR THE 1D CASE

The plasma has the tendency to remain electrically quasineutral, i.e., a net electric charge is effectively screened off by collective effects. The Coulomb electric field of a test charge vanishes outside a sphere whose radius is of the order of the Debye length, $\lambda_D = \sqrt{\epsilon_0 KT/2ne^2}$. In this study the Debye length is of the order of meters therefore much smaller than the characteristic scale length of density and field variations that are of the order of tens of kilometers in the collisionless plasma jet considered here. Therefore it can be assumed that the quasineutrality condition is very well satisfied in each point of the whole domain Γ. There are no strong double layers (or electrostatic shocks) nor contact discontinuity in the domain of integration. Thus the electrostatic potential is computed from the equation of quasineutrality, i.e.,

the condition that the total number of electrons is equal to the total number of positive charges:

$$\sum_{\alpha} \rho_{\alpha}(\Phi(y,z),A_x(y,z)) = 0, \tag{26}$$

where the summation takes place over the number of species (two in our case: electrons and protons). The analytical expressions of the charge densities, $\rho_{\alpha}(A_x(y,z),\Phi(y,z))$, are given by the expression (A2) in Appendix A. The nonlinear algebraic equation (26) conveniently replace the partial derivatives equation (15) in the system of equations that determines the distribution of the electromagnetic potentials. It is checked *a posteriori* that the neglected second order derivatives in Eq. (15) are indeed negligibly small (of the order of 10^{-3}, in the case of the normalized potential) for all solutions considered below.

Solution (13) of the Vlasov equation is a function of the spatial coordinates y and z via the electromagnetic potentials $\Phi(y,z)$ and $A_x(y,z)$. The Dirichlet boundary conditions for $A_x(y,z)$ (given in Table I) determine the spatial variation of both potentials; this determines then the VDF and the spatial distribution of all its moments, Q_{α}^{rst}. The variation of A_x with the z coordinate is controlled by the input boundary condition $A_{xL}(z)$:

$$\lim_{y \to -y_{\infty}} A_x(y,z) = A_{xL}(z) = B_0 y_{\infty} + \zeta(z). \tag{27}$$

As a result of this boundary condition at $y=-y_{\infty}$ the total magnetic field is, there, equal to the sum of the external B_0 and the small perturbation diamagnetic field: $b_{yL}(z)=d\zeta/dz$. On the other boundaries of the domain Γ we impose the condition that the magnetic field is uniform and equal to the external field, thus the magnetic vector potential is equal to $A_x=-B_0 y$ (see Table I).

The solution of the coupled equations (16) and (26) is computed numerically by an iterative method. First the equations are normalized such that all the quantities are nondimensional. The scaling factors are specified in Appendix B. Second the nondimensional equations are discretized on a 2D mesh with $N_y \times N_z$ points. Equation (26) is transformed then into $N_y \times N_z$ nonlinear algebraic equations. Equation (16) and its boundary conditions are transformed into a sparse linear system by a standard five-point Poisson method (see, e.g., Ref. [21]).

The initial guesses for $A_x(y,z)$ and $\Phi(y,z)$ are introduced into the expression of the charge density given in Eq. (A2). The latter is introduced into the discrete $N_y \times N_z$ nonlinear algebraic equations corresponding to Eq. (26). Each of the $N_y \times N_z$ nonlinear equations is solved by a bisection method giving the electric potential $\Phi(y,z)$ in each point of the mesh. This solution of the electric potential is then used to recompute the charge and current densities (A2) and (A4). The latter are introduced into the discrete equation (16) that is solved to find an updated solution for $A_x(y,z)$. The sparse linear system is solved with a pre-conditioned Gauss-Seidel method that converged after a reasonable number of steps. The electric charge and current densities given by Eqs. (A2) and (A5) are recomputed for the updated $A_x(y,z)$. The new electron and proton densities are introduced into the quasineutrality equation that is solved for an updated electric potential $\Phi(y,z)$. The procedure is repeated iteratively until the updating produces a change of each potential less than a given threshold ϵ. In the computations discussed in this and next section $\epsilon=10^{-6}$. The procedure converged in general in less than 50 iterations.

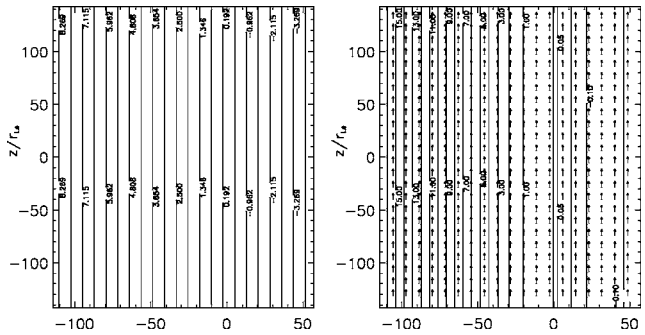

FIG. 3. Isocontours of the normalized magnetic vector potential A_x (left panel) and the normalized electrostatic potential $\Phi(y)$ (right panel). These results correspond to a one-dimensional tangential discontinuity parallel to the xOz plane, centered in $y=0$. The magnetic field lines are then straight lines parallel to the z direction as in the TD models of Sestero [6,8]; the arrows correspond to the magnetic field vectors $\boldsymbol{B}$; the magnetic field is everywhere parallel to the z axis and its magnitude has a small dip inside the discontinuity (i.e., for $y \in [-50,+50]$) where the diamagnetic current is enhanced, as can be seen from the upper left panel of Fig. 4.

The kinetic model and the numerical method described above have first been tested for a 1D tangential discontinuity which corresponds to the cases where the potentials and the plasma parameters are functions of y but do not vary with the z coordinate. The function $\zeta(z)$ is then equal to zero in the boundary condition (27). Figure 3 illustrates the iterated solutions obtained for $A_x(y)$ (left panel) and $\Phi(y)$ (right panel). The electromagnetic field does not depend on the z coordinate: the isocontours of Φ are straight lines aligned with z; furthermore, the diamagnetic perturbation of the B field has only one nonvanishing component, $\boldsymbol{b} \equiv (0,0,b(y))$, thus the magnetic field lines are everywhere parallel to the Oz axis as illustrated in Fig. 3.

The normalized distribution of the electric potential Φ/λ_{Φ}, density n/N_0, bulk velocity V_x/λ_V, and total electric current density J_x/λ_{J_x} vs y/λ_y are given in Fig. 4. The scaling factors $(N_0,\lambda_V,\lambda_{J_x},\lambda_y)$ and their values are specified in Table II. The distributions of the electric potential, current, density, and bulk velocity are similar to those obtained in the 1D-TD models by Sestero [8]. Indeed this trivial case corresponds to a tangential discontinuity in the Ox direction with a sheared convection whose velocity is V_0 on the left hand side of the TD, and equal to zero in the right hand side. There is no variation of the bulk velocity in the direction of the magnetic field in this trivial case which is used here as a test of our numerical method. The component of the electric field parallel to $\boldsymbol{B}$ (not shown) is everywhere equal to zero as in ideal MHD. The plasma density has a peak in the middle of the discontinuity.

Our results recover those obtained earlier by Sestero [8]. The TD model illustrated in Fig. 4 corresponds to a sharply

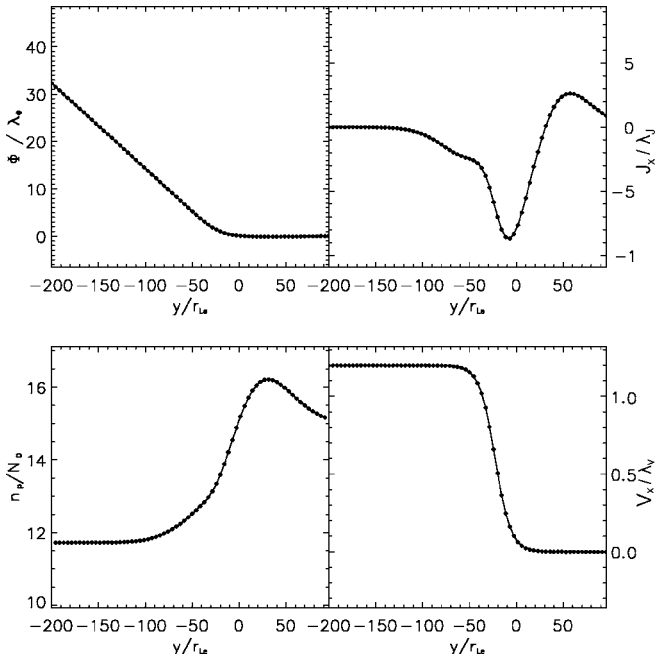

FIG. 4. Normalized plasma parameters and electrostatic potential across the tangential discontinuity illustrated in Fig. 3. Upper left panel: electric potential; upper right panel: total electric current density; lower left panel: proton density (equal to the electron density); lower right panel: plasma bulk velocity. All the quantities are normalized with the scaling factors defined in Appendix B.

sheared convection velocity called by Sestero an "electron rich" discontinuity. Our model reproduces also Sestero's smoother profiles (or "ion rich" discontinuities—not shown) by changing the direction of the convection velocity from V_0 to $-V_0$ at the left hand side boundary. This confirms an important result already obtained by Sestero [8].

V. NUMERICAL RESULTS FOR 2D SHEARED FLOW: AN EXAMPLE

A number of numerical simulations based on the model and method described above were performed for various boundary conditions and plasma parameters. In the remainder of this paper we discuss only one example that, however, shows key elements which are common to all our simulations. Additional numerical solutions are discussed by Echim [12].

Let us recall that the solution discussed here have to satisfy two conditions: (i) the variations of the fields are smooth such that the magnetic moment is adiabatically conserved and (ii) the B_z component of the total magnetic induction (including diamagnetic perturbation) is significantly stronger than B_y such that the definition (4) of μ_α holds true. Therefore the results are confined in a region symmetric with respect to the $y=0$ axis, where strong boundary effects are negligible.

The input parameters used in this example are given in Table II. They have values typical for the plasma flow at the interface between the solar wind and the terrestrial magnetosphere. The plasma beta is very small, $\beta=1.38\times10^{-6}$. As a matter of consequence the diamagnetic currents produce relatively small magnetic perturbations compared to the external field, $\boldsymbol{B}_0$. This corresponds to the cold plasma approximation, with the electrons having greater temperature than the protons, $T_e>T_p$. In the example discussed here the ratio between the average Larmor radii of the protons and electrons is equal to $r_{Lp}/r_{Le}=13$. All the results illustrated graphically below are given in nondimensional units, the scaling factors are defined in the Appendix B and given in Table II.

The variation of $A_x(z)$ imposed at the left hand side border is determined here by the *ad hoc* function:

$$\zeta(z)=\Theta_1\,\mathrm{erfc}\left(\frac{z^2-z_{\mathrm{lim}}^2}{z_c^2}\right), \tag{28}$$

where Θ_1, z_c, and $z_{\mathrm{lim}}<z_\infty$ are three positive constants. Note that this choice is not critical and can easily be changed to fit for instance an observed magnetic field distribution in a moving plasma jet or plasmoid. The parameter Θ_1 corresponds to the amplitude of the z dependent perturbation of $A_x(z)$; z_{lim} determines the limits of the region within which the perturbation is largest; and z_c determines the half width of the transition region where B_y changes from 0 to $d\zeta/dz$ [see Eq. (27)]. The choice of the complementary error function (erfc) does not restrict in any way the generality of the numerical solution. Indeed, any alternative function, symmetric or not in z, can be adopted. The results discussed below are obtained for $\Theta_1=(B_0/2)y_\infty$, $z_{\mathrm{lim}}=100r_{Le}$, and $z_c=10r_{Le}$.

The left panel of Fig. 5 shows the final (iterated) solution of Eq. (16) with boundary conditions specified in Table I. The limits of the domain of integration Γ are equal to $\pm y_\infty=\pm z_\infty=\pm150r_{Le}$ in our example: we have checked that the results do not critically depend on this assumption. The field distributions are only shown for $y/r_{Le}\in[-70,+90]$, i.e., in the vicinity of the plane $y=0$. $A_x(y,z)$ is mainly determined by the boundary conditions since the internal diamagnetic electric current density is small. In the 3D space, the iso-contours of A_x correspond to curved surfaces parallel to the Ox axis. They give a magnetic field whose main component is B_z and has a small b_y mainly due to the perturbation $\zeta(z)$ imposed at the left hand side edge and propagated

TABLE II. Boundary values, scaling factors, and their physical units, used as input parameters in the numerical solutions discussed in Sec. III and illustrated in Figs. 3–10 ($N_{e1}=N_{e2}$, $T_{e1}=T_{e2}$, $T_{p1}=T_{p2}$).

B_0 (nT)	N_0 (cm^{-3})	N_{e1} (cm^{-3})	N_{p1} (cm^{-3})	N_{p2} (cm^{-3})	T_{ref} (eV)	T_{e1} (eV)	T_{p1} (eV)	V_0 (km/s)	λ_D (m)	r_{Le} (m)	λ_B (nT)	λ_Φ (V)	λ_V (km/s)	λ_E (mV/m)	y_∞ (km)	z_∞ (km)
75	1	15	15	1	1	15	1.5	700	7.4	180	10^3	1	500	5.5	35	35

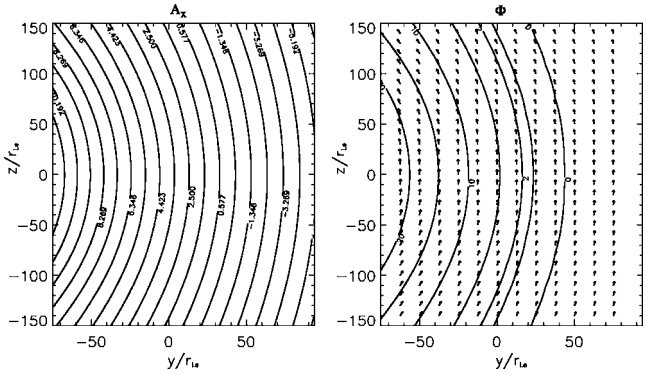

FIG. 5. Solution of the coupled system of Eq. (16) and (26) obtained by the iterative procedure. The two panels show, respectively, isocontours of the normalized magnetic vector potential component A_x (left panel) and the normalized electric potential Φ (right panel). The arrows correspond to the projections of the magnetic field vectors in any plane perpendicular to the plasma stream velocity, i.e., perpendicular to the Ox axis.

inside the domain Γ. The comparison of Figs. 3 and 5 illustrates how A_x changes when the boundary condition is changed from $\zeta(z)=0$ to the expression (28).

The electrostatic potential $\Phi(y,z)$, computed from the quasineutrality equation (26), is given in the right panel of Fig. 5. The equipotential surfaces are curved surfaces parallel to the Ox axis; their intersection with the yOz plane is shown in the right panel. Φ decreases smoothly from its maximum value at the left hand side edge, $y=-y_\infty$. It has an increased gradient in the region centered at $y=0$, extending roughly from $y=-30\ r_{Le}$ to $y=+50\ r_{Le}$. This region of transition, forming at the interface between the fast moving plasma jet and the background stagnant plasma will be called the boundary layer (BL). The electric potential is equal to zero in the region of stagnant plasma, i.e., for $y>50r_{Le}$. The electric field corresponding to the electrostatic potential is discussed below. Note that a close inspection of the equipotentials of Φ and the isocontours of A_x reveals the misalignment between the two.

The isocontours of the magnetic field intensity are displayed in the left panel of Fig. 6; it shows the distribution of $|\boldsymbol{B}|$ in any of the planes perpendicular to the Ox axis and to the bulk velocity of the plasma jet. The intensity of $\boldsymbol{B}$ decreases smoothly from its maximum value imposed on the left hand boundary, $y=-150r_{Le}$, to the value of the background magnetic field, on the right hand side.

The isocontours in the right panel of Fig. 6 correspond to constant values of the plasma jet bulk velocity, $V_x(y,z)$. Note that by definition $V_y=V_z=0$ in this first type model for a sheared plasma flow. The jet plasma is indeed restricted to drift parallel to the Ox axis, normal to the magnetic field direction. However, its bulk velocity V_x changes along magnetic field lines as will be discussed below. The jet plasma bulk velocity has a maximum value of 550 km/s at the left hand side (at $y=-y_\infty$). The bulk velocity is roughly constant in the core of the plasma jet, i.e., for $y<-30r_{Le}$. It decreases inside the boundary layer from 550 km/s to roughly $V_x=0$ for $y>50$. Inside the boundary layer the plasma bulk velocity varies both with the y and z coordinates as sketched in Fig. 1.

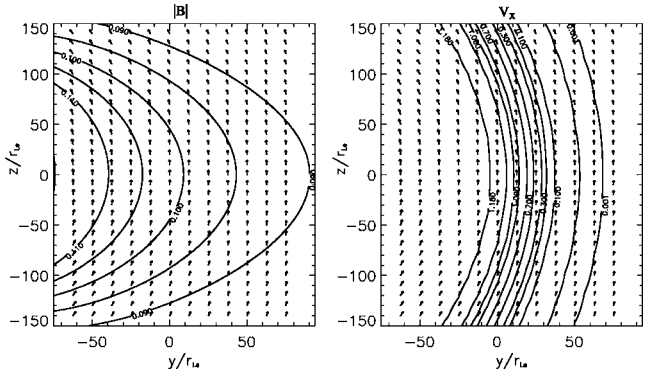

FIG. 6. Left hand side panel shows the distribution of the isocontours of the normalized magnetic field intensity $B(y,z)$. Right hand side panel shows the distribution of isocontours of the normalized plasma bulk velocity field $V_x(y,z)$. The maximum of the velocity in physical units is equal to 550 km/s. The arrows correspond to the projections of the magnetic field vectors in any plane perpendicular to the plasma stream velocity, i.e., perpendicular to the Ox axis.

The isocontours of the bulk velocity do not coincide with the isocontours of $A_x(y,z)$ nor with those of constant $\Phi(y,z)$. This misalignment implies that the different points of the same field line do not "convect" with the same velocity as assumed in ideal MHD. There is also a misalignment between the lines of equal electric potential and the magnetic field lines. This implies that the magnetic field lines are not electric equipotentials as postulated in the ideal MHD approximation of plasma physics.

The left panel of Fig. 7 shows the lines of equal values of $|\boldsymbol{E}_\perp|$, the modulus of the perpendicular component of the electric field. In the right hand side panel the isocontours of $E_\parallel$, the parallel component, are displayed. The perpendicular component of the electric field decreases slightly inside the plasma jet ($y<-40r_{Le}$). Inside the boundary layer the per-

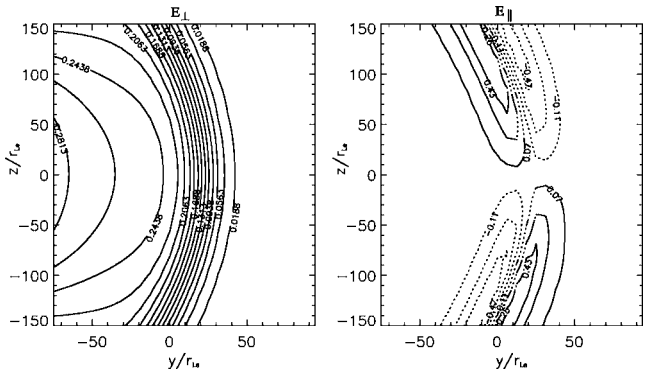

FIG. 7. Left panel: isocontours of the perpendicular component of the normalized electric field; the maximum value of $E_\perp$ (in physical units) is equal to 1.54 mV/m. Right panel: isocontours of $E_\parallel$, the parallel component of the normalized electric field. The solid contours correspond to positive values while the dotted contours correspond to negative values. The values (in physical units) of parallel E field range from $-3.67\ \mu$V/m to $+3.87\ \mu$V/m with steps of $0.04\ \mu$V/m. In the ideal MHD approximation of plasma physics $E_\parallel=0$.

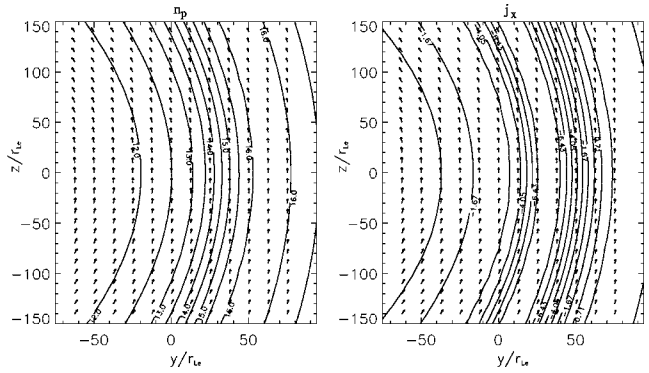

FIG. 8. Left panel: isocontours of n_p, the normalized density of protons; n_p is equal to n_e (the electron density) since Eq. (26) is satisfied in the system. The maximum of the particle density (in physical units) is equal to 11.83 cm^{-3}. Right panel: isocontours of $j_x(y,z)=j_{xp}(y,z)+j_{xe}(y,z)$, the normalized total electric current; the current takes value between -6.4 $\mu A/m^2$ and $+3.2$ $\mu A/m^2$. In both panels the arrows illustrate the local inclination and amplitude of the total magnetic field.

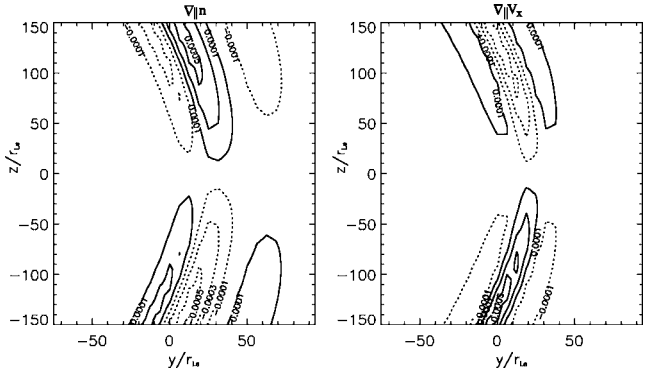

FIG. 9. Left hand side panel: isocontours of $\nabla_\parallel n$, the normalized parallel gradient of the proton and electron densities. The values of $\nabla_\parallel n$ (in physical units) range from -2.5 m^{-4} to $+2.5$ m^{-4} by steps of 0.5 m^{-4}. Right hand side panel: isocontours of $\nabla_\parallel V_x$, the normalized parallel gradient of the plasma bulk velocity. The values of $\nabla_\parallel V_x$ vary from -1.5 s^{-1} to $+1.5$ s^{-1} by steps of 0.25 s. In both panels the solid contours correspond to positive values while the dotted contours correspond to negative values.

pendicular E field decreases from 1.13 mV/m to 0.09 mV/m. The electric drift, $\boldsymbol{U}_E(y,z)=\boldsymbol{E}_\perp\times\boldsymbol{B}/B^2$ is parallel to the x direction as is the plasma bulk velocity V_x. The parallel component of the E field is equal to zero inside the jet as well as in the background stagnant plasma. It takes, however, finite values inside the boundary layer. The maximum of $E_\parallel$ is of the order of several μV/m, i.e., orders of magnitude smaller than the perpendicular component. Nevertheless, parallel electric fields are extremely efficient in generating field aligned currents, indeed the conductivity along magnetic field is very high in collisionless plasmas.

The left hand side panel of Fig. 8 shows the isocontours of the proton density. Since the quasineutrality is satisfied [Eq. (26)] the same isocontour lines correspond to the density of electrons. The density is uniform inside the plasma jet ($y<-40r_{Le}$). It increases inside the BL and then smoothly decreases to its asymptotic values at large distances on both sides of the BL. The right hand side panel shows the isocontours of $j_x(y,z)=j_{xp}(y,z)+j_{xe}(y,z)$, the total current density. The electric current is vanishingly small near the center of the plasma jet. Inside the BL the current is nonzero and changes sign from negative values (with a maximum equal to -6.4 $\mu A/m^2$ to positive values (with a maximum equal to $+3.2$ $\mu A/m^2$). The current density tends also to zero at large distances outside the BL, in the region of stagnant plasma. It is this small electric current density that is responsible for the small diamagnetic effect observed in the distribution of the magnetic induction, $\boldsymbol{B}(y,z)$.

The key new feature of our 2D boundary layer (BL) is the nonvanishing parallel electric field, i.e., $\boldsymbol{E}\cdot\boldsymbol{B}\neq 0$. The distribution of $E_\parallel$ indicates that the boundary layer of the plasma jet, where the shear of the velocity is maximum, is precisely the site of an electric potential gradient similar to that observed for weak double layers (*WDL*) in laboratory and space experiments [22–26]. Indeed the right hand side of Fig. 7 displays two adjacent pairs of *WDL*-like structures with reversed polarities. The region of parallel electric field extends all along the boundary layer. Detailed plots of field aligned electric field are shown in the lower left hand side panel of Fig. 10 for four different values of y. The parallel component of the electric field reaches a maximum value equal to 4 μV/m at $z/r_{Le}\approx\pm 100$.

The origin of this parallel electric field component can be elucidated by a detailed analysis of the 2D distributions of the electron density and plasma bulk velocity. Indeed, although in Fig. 8 the lines of constant proton and electron densities seem to parallel the direction of the magnetic field vectors, a closer inspection indicates, however, that ∇n, the gradient of the density, has a nonzero component parallel to the magnetic field lines. The isocontours of $\nabla_\parallel n$, illustrated in the left hand side panel of Fig. 9, indicate the formation of adjacent layers inside of BL where $\nabla_\parallel n$ is finite and changes sign.

The right hand side panel of Fig. 9 displays isocontours of $\nabla_\parallel V_x$, the gradient of the plasma bulk velocity in the direction of the magnetic field lines. This quantity corresponds to the parallel component of the velocity shear; it is equal to zero ($\nabla_\parallel V_x=0$) in ideal MHD. The distribution of $\nabla_\parallel V_x$ is equal to zero in the central regions of the plasma jet as well as in the stagnant plasma. Inside the BL two adjacent regions with finite $\nabla_\parallel V_x$ are formed. Within these regions the bulk velocity is significantly sheared and $\nabla_\parallel V_x$ reverses sign. The sign of $\nabla_\parallel V_x$ correlates very well with the distribution of $E_\parallel$, plotted in the right hand side panel of Fig. 7; it anticorrelates with the sign of $\nabla_\parallel n$. This effect is evident in the lower panels of Fig. 10 showing the z profiles for a set of four values of y. Note the similitude of the dotted lines in both panels corresponding to $y=-12.5r_{Le}$. A detailed study of the relationship between $E_\parallel$, $\nabla_\parallel n$, and $\nabla_\parallel V_x$ has been given in Ref. [12].

VI. SUMMARY AND CONCLUSIONS

Sestero's one-dimensional model [8] of a tangential discontinuity with plasma velocity sheared in the direction per-

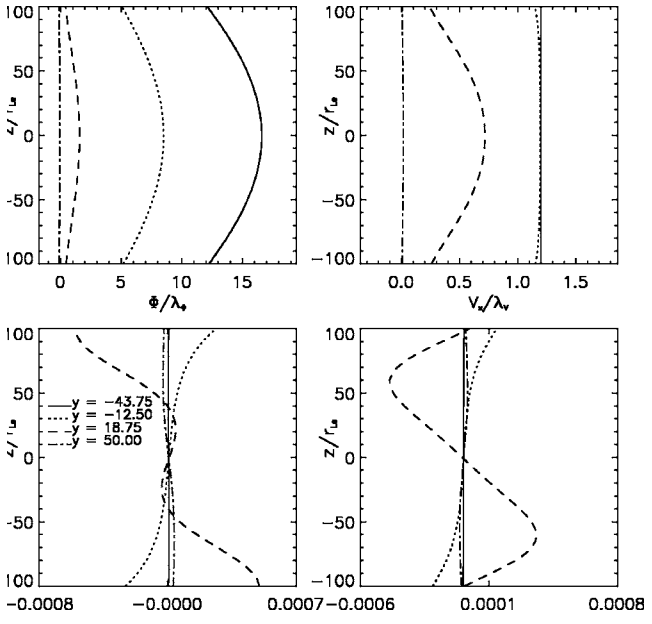

FIG. 10. The z profile of the nondimensional electrostatic potential (upper left panel), plasma bulk velocity (upper right panel), parallel component of the electric field (lower left panel), and parallel gradient of the plasma bulk velocity (lower right panel). The plots correspond to four different y coordinates given in the lower left panel.

pendicular to the magnetic field lines has been extended to take into account a shear parallel to the magnetic field lines: $\nabla_{\perp} V_x \neq 0$ and $\nabla_{\parallel} V_x \neq 0$. A two dimensional, steady-state model has been developed here by adding to Sestero's 1D model a gradient of the electric and magnetic fields, $\boldsymbol{E}(y,z)$ and $\boldsymbol{B}(y,z)$, and plasma variables, $V_x(y,z)$ and $n(y,z)$, in the direction parallel to the magnetic field direction. The velocity distribution function of each plasma species (electrons and protons) has been expressed in terms of two constants of motion. A third constant of motion, needed to determine the moments of the VDF, has been approximated by the magnetic moment, an adiabatic invariant. This approximation imposes certain constraints on the stationary model developed here. The spatial variation of the VDF is introduced through boundary conditions imposed on the magnetic vector potential, $A_x(y,z)$, i.e., the function $\zeta(z)$ defined by Eq. (28).

The electric field is determined by an electrostatic potential $\Phi(y,z)$ which is obtained by solving the quasineutrality equation (26). The magnetic field distribution is determined by a vector potential $A_x(y,z)$ by solving the Maxwell-Ampere equation (16). The example discussed in Sec. V illustrates numerically the main features of our kinetic model for 2D plasma jets whose convection velocity is sheared both in the direction parallel and perpendicular to the magnetic field. The transition between a fast plasma jet and a background stagnant plasma takes place within a 2D boundary layer. As a result of small diamagnetic currents the magnetic field lines are slightly curved. The plasma bulk velocity is nearly uniform in the center of the jet; its value V_x is slightly different from the MHD convection velocity, $U_E = E_{\perp}/B$. The bulk velocity decreases within a boundary layer (BL) where it changes from a maximum value, $V_x = V_0$, in the inner jet to $V_x = 0$ at large distance on the right hand side, in the stagnant plasma region. The bulk velocity within the boundary layer can no more be approximated by the ideal MHD convection velocity U_E.

An interesting feature is the nonvanishing parallel (or magnetic field aligned) component of the electric field. The parallel E fields are localized inside the BL; they are almost equal to zero near the center of the jet as well as in the background stagnant plasma. The magnitude of the parallel electric field is anticorrelated with the parallel gradient of the electron density ($\nabla_{\parallel} n$) and correlated with the parallel gradient of the plasma bulk velocity ($\nabla_{\parallel} V_x$). It is this non-MHD parallel electric field that allows the plasma from different parts of the magnetic field tubes to drift with different convection velocities.

Parallel electric fields are neglected in ideal MHD where $\boldsymbol{E} \cdot \boldsymbol{B} = 0$. The contribution of $\nabla_{\parallel} V_x$ in producing a parallel electric field has been determined quantitatively in this paper. The numerical algorithm developed to solve the coupled equations that describe the electromagnetic field converges well for the input parameters illustrated in this study. Our kinetic model gives a reasonable solution for non-MHD 2D boundary layers forming at the edges of plasma jets moving through background magnetic field and stagnant plasma.

ACKNOWLEDGMENTS

This work was supported by the Belgian Federal Office for Scientific, Technical and Cultural Affairs through ESA PRODEX/Cluster. M.M.E. thanks Dr. M. Roth for many discussions concerning the TD models and acknowledges the support of the Romanian Space Agency.

APPENDIX A: MOMENTS OF VELOCITY DISTRIBUTION FUNCTION

The electric charge and current density are proportional respectively to the zero order and first order moment of the VDF. Their analytical expressions are obtained by integrating the velocity distribution function defined in Eq. (11) and (13). The number density of the species α is determined by

$$Q_{\alpha}^{000} = 4 \int_{-\infty}^{+\infty} \int_{H_{c\alpha}}^{+\infty} \int_{\mu_{c\alpha}}^{+\infty} \left[\frac{\sqrt{B} f_{\alpha}(H,\mu,p_x)}{2m_{\alpha}^2 \sqrt{H - H_{c\alpha}} \sqrt{\mu - \mu_{c\alpha}}} \right] dH d\mu dp_x. \tag{A1}$$

Using the expressions (7), (8), (11), and (13) the integrals (A1) can be expressed in terms of analytical functions. The zero order moment is proportional to the charge density:

$$\rho_{\alpha}(y,z) = \frac{q_{\alpha} N_{\alpha 1}}{2} e^{-e\Phi(y,z)/KT_{\alpha 1}} \operatorname{erfc}\left(\frac{eA_x(y,z)}{\sqrt{2m_{\alpha} KT_{\alpha 1}}} \right) + \frac{q_{\alpha} N_{\alpha 2}}{2} e^{[-e\Phi(y,z) - eA_x(y,z)V_0]/KT_{\alpha 2}} \times \operatorname{erfc}\left(- \frac{eA_x(y,z)}{\sqrt{2m_{\alpha} KT_{\alpha 2}}} \right). \tag{A2}$$

The electric current density of the species α is determined by

the first order moments of the VDF. Only Q_α^{100} is different from zero:

$$Q_\alpha^{100} = 4\int_{-\infty}^{+\infty}\int_{H_{c\alpha}}^{+\infty}\int_{\mu_{c\alpha}}^{+\infty}\left(\frac{p_x - q_\alpha A_x}{m_\alpha}\right) \times\left[\frac{\sqrt{B}f_\alpha(H,\mu,p_x)}{2m_\alpha^2\sqrt{H-H_{c\alpha}}\sqrt{\mu-\mu_{c\alpha}}}\right]dHd\mu dp_x. \quad \text{(A3)}$$

Using the expressions (7), (8), (11), and (13) the electric current density becomes

$$j_{x\alpha}(y,z) = N_{\alpha 2}\sqrt{\frac{KT_{\alpha 2}}{2\pi m_\alpha}}e^{-e[\Phi(y,z)-A_x(y,z)V_0]/KT_{\alpha 2}} \times\left[\sqrt{\frac{\pi m_\alpha}{2KT_{\alpha 2}}}V_0\,\mathrm{erfc}\left(-\frac{eA_x(y,z)}{\sqrt{2m_\alpha KT_{\alpha 2}}}\right) + b_\alpha e^{(eA_x)^2/2m_\alpha KT_{\alpha 2}}\right] - b_\alpha N_{\alpha 1}\sqrt{\frac{KT_{\alpha 1}}{2\pi m_\alpha}}e^{-e\Phi(y,z)/KT_{\alpha 1}} \times e^{-[eA_x(y,z)]^2/2m_\alpha KT_{\alpha 1}}, \quad \text{(A4)}$$

$$j_{y\alpha}(y,z) = 0, \quad j_{z\alpha}(y,z) = 0, \quad \text{(A5)}$$

where $b_\alpha = \mathrm{sgn}(q_\alpha)$. It should be pointed out that our choice of truncated Maxwellian VDF (7), (8), and (11) is dictated by mathematical convenience, not by any basic physical reason. For any more complex VDF derived from particle flux experimental measurements, the triple integrals (A1) and (A3) would have to be calculated by more evolved numerical integrations.

APPENDIX B: SCALING FACTORS

For convenience all plasma and electromagnetic field variables have been normalized. The general rule of normalization is defined by

$$P = \lambda_P P^*,$$

where P is the physical quantity, λ_P is the dimensional scaling factor, and P^* is the corresponding nondimensional quantity.

The electric potential is scaled with the potential difference necessary to accelerate an electron to a thermal reference energy KT_{ref}:

$$\Phi = \lambda_\Phi \Phi^*, \quad \lambda_\Phi = \frac{KT_{ref}}{e}.$$

The magnetic vector potential is scaled with

$$A_x = \lambda_{A_x} A_x^*, \quad \lambda_{A_x} = \frac{\sqrt{2m_e KT_{ref}}}{e}$$

and the electric current with

$$\boldsymbol{j} = \lambda_j \boldsymbol{j}^*, \quad \lambda_j = (eN_0)\sqrt{\frac{2KT_{ref}}{m_e}}.$$

The velocity is scaled with the electron thermal velocity

$$V = \lambda_V V^*, \quad \lambda_V = \sqrt{\frac{2KT_{ref}}{m_e}};$$

we have also defined the nondimensional quantities

$$\gamma = \frac{m_e}{m_i}, \quad \tau_e = \frac{T_{ref}}{T_{e1}}, \quad \tau_{e2} = \frac{T_{ref}}{T_{e2}},$$

$$\tau_i = \frac{T_{ref}}{T_{i1}}, \quad \tau_{i2} = \frac{T_{ref}}{T_{i2}}.$$

The spatial coordinate perpendicular and parallel to the magnetic field are both scaled with the electron Larmor radius,

$$y = \lambda_y y^*, \quad \lambda_y = \frac{\sqrt{2m_e KT_{ref}}}{eB},$$

$$z = \lambda_z z^*, \quad \lambda_z = \frac{\sqrt{2m_e KT_{ref}}}{eB}.$$

The values of these scale factors are given in Table II for the plasma jet model discussed above.

[1] R. Lundin *et al.*, Ann. Geophys. **21**, 457 (2003).
[2] J. Lemaire, J. Plasma Phys. **33**, 425 (1985)
[3] H. W. Emmons and R. I. Lamd, Phys. Fluids **5**, 1489 (1962).
[4] N. Brenning and C.-G. Fälthammar, Phys. Scr. **70**, 153 (2004).
[5] S. I. Krasheninnikov, Phys. Lett. A **283**, 368 (2001).
[6] A. Sestero, Phys. Fluids **7**, 44 (1964).
[7] J. Lemaire and L. F. Burlaga, Astrophys. Space Sci. **45**, 303 (1976).
[8] A. Sestero, Phys. Fluids **9**, 2006 (1966).
[9] M. Roth, J. Atmos. Terr. Phys. **38**, 1065 (1976).
[10] M. Roth, J. De Keyzer, and M. Kuznetsova, Space Sci. Rev. **76**, 251 (1996).
[11] L. C. Lee and J. R. Kan, J. Geophys. Res. **84**, 6417 (1979).
[12] M. M. Echim, Ph.D. thesis, Université Catholique de Louvain, Louvain-la-Neuve, 2004 (http://edoc.bib.ucl.ac.be:81/ETD-db/collection/available/BelnUcetd-06292004-182139/).
[13] J. L. Delcroix and A. Bers (in French), *Physique des plasmas*, Savoirs Actuels (InterÉditions/CNRS Éditions, Paris, 1994).
[14] H. Alfvén, *Cosmical Electrodynamics* (Clarendon Oxford, 1953).
[15] T. G. Northrop, *The Adiabatic Motion of Charged Particles* (Interscience, New York, 1963).
[16] J. Lemaire and M. Scherer, Phys. Fluids **14**, 1683 (1971).
[17] J. Lemaire and M. Scherer, Rev. Geophys. Space Phys. **11**, 2, 427, (1973).
[18] V. Pierrard and J. Lemaire, J. Geophys. Res. **101**, 7923 (1996).

[19] E. C. Whipple, J. Geophys. Res. **82**, 1525 (1977).
[20] M. W. Liemohn and G. V. Khazanov, Phys. Plasmas **5**, 580 (1998).
[21] P. M. Morse and H. Feshbach, *Methods of Theoretical Physics* (McGraw-Hill, New York, 1953).
[22] M. A. Raadu, Phys. Rep. **178**, 25 (1989).
[23] C. L. Longmire, *Elementary Plasma Physics* (Interscience, New York, 1963).
[24] M. Temerin, K. Cerny, W. Lotko, and F. S. Mozer, Phys. Rev. Lett. **48**, 1175 (1982).
[25] A. J. Hull, J. W. Bonnell, F. S. Mozer, J. D. Scudder, and C. C. Chaston, J. Geophys. Res. **108**, 1265 (2003).
[26] T. Hurtig, N. Brenning, and M. A. Raadu, Phys. Plasmas **10**, 4291 (2003).